

Molecular Layer Deposition of Alucone Thin Film on LiCoO₂ to Enable High Voltage Operation

Ortal Lidor-Shalev,^[a] Nicole Leifer,^[a] Michal Ejgenberg,^[a] Hagit Aviv,^[a] Ilana Perelshtein,^[a] Gil Goobes,^{*[a]} Malachi Noked,^{*[a]} and Rosy^{*[a, b]}

Extracting the theoretically high capacity of LiCoO₂ (LCO) is desirable for enhancing the energy density of currently used lithium-ion batteries (LIBs) for portable devices. The bottleneck for exhibiting the high capacity is associated with the limited cut-off positive voltages beyond which degradation of electrode/electrolyte takes place. In this work, we apply hybrid organic-inorganic alucone thin film grown directly on LCO by a molecular layer deposition (MLD) method, using sequential

exposure to Al-based and organic-based precursors. The alucone thin films enabled the high voltage operation of the LCO cathode (>4.5 V), acting as a protection layer. Electrochemical studies proved that alucone coated LCO show enhanced electrochemical performances with improved cycling stability and enhanced specific capacity, relative to uncoated LCO. Amongst the studied films, 10 nm ethylene glycol/Al coated LCO have shown the best results.

1. Introduction

Lithium-ion batteries (LIBs) are the state-of-the-art electrochemical energy storage technology for mobile electronic devices and electric vehicles.^[1,2] Accordingly, with high theoretical capacity and energy density, the LIBs have attracted a continuously increasing interest.^[3–5] To further improve the energy density and reduce the cost of LIBs, tremendous efforts have been devoted for developing new improved materials.^[6,7]

Lithium cobalt oxide, LiCoO₂ (LCO), is the most veteran and dominant cathode material in the mobile electronics market even after nearly 30 years.^[8–10] The LCO cathode holds a high theoretical specific capacity of 274 mAh/g and a high volumetric energy density. However, cycling LCO-based batteries to voltages greater than 4.35 V vs. Li/Li⁺ causes significant structural instability and severe capacity fade.^[11,12] The critical problems of LCO cathodes focus on surface degradation, damages induced by damaging phase transitions, O₂ loss, Co dissolution, and inhomogeneous reactions.^[13] Various strategies have been proposed to overcome those issues and promote the long-cycling stability at high voltage, amongst which are element doping,^[14] commodification approaches,^[15,16] sol precursors with further calcination,^[17] and fabrication of 3D cells.^[18] Another approach to effectively protect the electrode surface is

surface coating^[19–23] by a solid lithium ion conductive barrier sited between the electrode and the electrolyte surfaces. Such a passivation layer optimizes the surficial electrode structure, promotes surface charge transfer, limits the transition metal ions dissolution, controls interfacial response, and enhances the cell kinetics. Among the coating methods, atomic layer deposition (ALD)^[24–28] is ideal for producing thin films with a controllable, conformal and uniform design by sequential self-limited reactions. Previous works have demonstrated ALD as a viable technique to modify electrodes with different inorganic metal oxides thin films,^[29–33] including Al₂O₃, TiO₂, and ZrO₂ thin film coatings. Such ALD thin films are used as an artificial solid electrolyte interphase (ASEI) that improves the electrodes stability enhances their electrochemical performance.^[34]

Molecular layer deposition (MLD),^[35,36] the organic analogy of ALD, similarly provides precise control over the coating thickness and composition in a conformal growth.^[37,38] While the ALD processes are usually limited to inorganic metal-oxides/nitrides/sulfides/phosphate and metal-films, the MLD can produce pure polymeric thin films and hybrid organic-inorganic thin films of organic ligand linked by metal ion linker.^[39–44] Previous works have described the MLD of different hybrid organic-inorganic thin films using precursors of diethyl zinc (DEZn) or trimethylaluminum (TMA) as the sources for metal layer, and hydroquinone(HQ), ethylene glycol (EG) or their derivatives as the organic precursors.^[45–52] The thin films produced by ALD and MLD hold further advantages such as lower growth temperatures, tunable thermal stability, and improved mechanical properties. The unique capability of MLD to conformal coat electrodes by thin films enables the formation of stable passivation layers. Such protection coatings prevent electrode materials from degradation at low/high electrochemical potentials, while facilitating the flux of ions across interfaces, with increased mechanical flexibility.^[53,54]

In this paper, we have produced alucones thin films by MLD to effectively coat LCO cathode with a conformal artificial

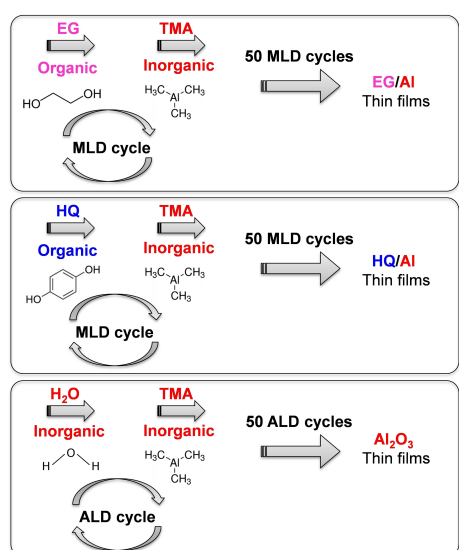
[a] Dr. O. Lidor-Shalev, Dr. N. Leifer, Dr. M. Ejgenberg, Dr. H. Aviv, Dr. I. Perelshtein, Prof. G. Goobes, Prof. M. Noked, Dr. Rosy
Department of Chemistry
The Institute for Nanotechnology, Advanced Materials Bar-Ilan University
Ramat-Gan, Israel, Ramat Gan, 5290002, Israel
E-mail: Malachi.Noked@biu.ac.il
gil.goobes@biu.ac.il

[b] Dr. Rosy
Department of Chemistry
Indian Institute of Technology (Banaras Hindu University)
Varanasi, 221005, India
E-mail: roschy@iitbhu.ac.in

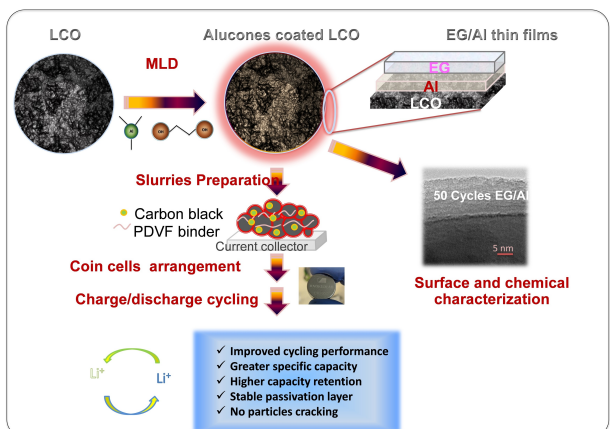
 Supporting information for this article is available on the WWW under
<https://doi.org/10.1002/batt.202100152>

cathode electrolyte interphase (CEI), to improve the cathode electrochemical performances. With in-depth characterization, we demonstrate the growth of alucones thin films having the composition of poly(aluminum ethylene glycol) and poly(aluminum hydroquinone), using sequential exposures of TMA and EG or HQ, respectively. The MLD alucones thin films were grown as passivation layers of ethylene glycol/Al (EG/Al) or hydroquinone/Al (HQ/Al) coatings. We focus our study on three types of thin films, as described in Scheme 1; (1) 50 MLD cycles of EG and TMA precursors for growth of EG/Al thin films; (2) 50 MLD cycles of HQ and TMA precursors for growth of HQ/Al thin films; and compare these 2 with (3) 50 ALD cycles of TMA and water precursors for growth of Al_2O_3 thin films.

Scheme 2 describes our strategy of work. After the MLD thin films were grown, they were characterized using nano-surface analyses and chemical characterization to prove a successful MLD growth. Next, the coated LCO were prepared as slurries and were assembled into coin cells, as described in the



Scheme 1. Schematic illustration of the thin films' growth by atomic and molecular layer deposition proposed in this work.



Scheme 2. Graphical description of our work methodology.

experimental section. And the next step, the electrochemistry performance and charge/discharge cycling of the alucones coated LCO and uncoated LCO were extensively studied.

2. Results and Discussion

Figure 1 depicts the high resolution transmission electron microscopy (HRTEM) and energy-dispersive X-ray spectroscopy (EDAX) analysis of EG/Al and HQ/Al thin film grown on LCO. As shown in Figure 1(a), the surface of the pristine LCO particle was uniform and homogenous, showing no coating over the LCO surface. Moreover, no Al atoms were detected from the surface of the LCO particles, as shown in EDAX (Figure 1a, bottom). With 50 repeated MLD cycles of EG/TMA, a coating with an average thickness of $\sim 10 \text{ nm} \pm 1 \text{ nm}$ (Figure 1b) was observed, indicating growth per cycles (GPC) of $\sim 0.2 \text{ nm}$ at 135°C . EDAX of the coating layer confirmed the presence of Al atoms (Figure 1b, bottom). 50 MLD cycles of HQ/TMA produces a coating with an average thickness of $\sim 11 \text{ nm} \pm 2 \text{ nm}$ (Figure 1c) with a well-ordered arrangement over the LCO surface, indicating growth per cycles (GPC) of $\sim 0.22 \text{ nm}$ at 150°C . EDAX of the coating layer confirmed the presence of Al atoms, demonstrating successful MLD growth of alucone films (Figure 1c, bottom).

For the ALD of Al_2O_3 thin film, TEM images reveal successful growth of coating with an average thickness of $11 \text{ nm} \pm 3 \text{ nm}$ (average GPC of 0.14 nm at 200°C , calculated from 80 ALD cycles) (Figure S11). EDAX of the coating layer further confirmed the presence of Al atoms, demonstrating successful ALD growth of Al_2O_3 (Figure S11, bottom).

Next, to examine the composition and chemical environment of the species in the alucone thin film, X-ray photo-electron spectroscopy (XPS) was employed. The $\text{Al}2p$ XPS scans for the EG/Al and HQ/Al coated LCO are depicted in Figure 2(a). As expected, the $\text{Al}2p$ peak was observed only in the coated

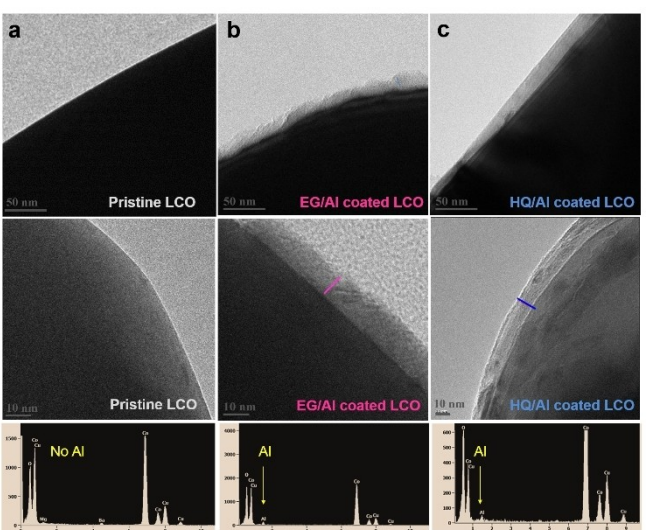


Figure 1. HRTEM images and EDAX (bottom) of; (a) pristine LCO; (b) 50 MLD cycles of EG/Al coated LCO; and (c) 50 MLD cycles of HQ/Al coated LCO.

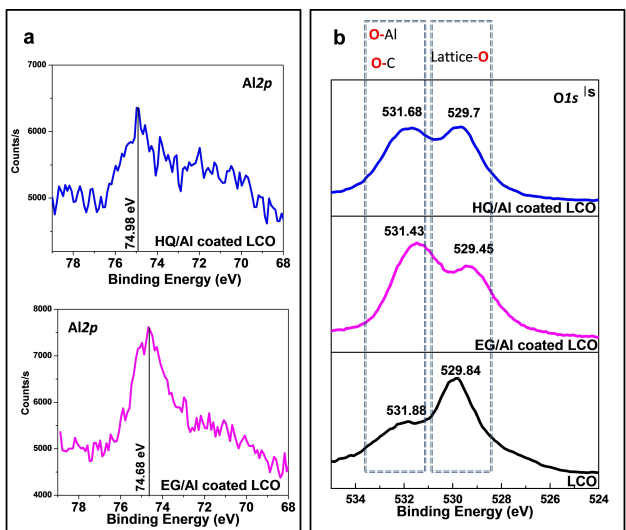


Figure 2. XPS spectra of (a) Al_{2p} scan and (b) O_{1s} scan, for alucone coated and uncoated LCO. Curves colors: uncoated LCO (black), EG/Al coated LCO (pink), and HQ/Al coated LCO (blue).

LCO samples, clearly indicating the deposition of Al containing thin films grown by MLD. The presence of any possible Al impurity in the uncoated LCO particles was also ruled out with the absence of any Al_{2p} peak in the uncoated LCO. The observed Al_{2p} peak at binding energies (BE) of ~75 eV corresponds to sub-stoichiometric AlO_x.^[55]

As shown in Figure 2(b), the O_{1s} spectra of the pristine LCO and both the alucones coated LCO samples are different. The O_{1s} spectra of the samples is composed of two O_{1s} peaks; one at BE of ~529 eV, associated with O atoms assigned to the LiCoO₂ lattice-O; and another peak at ~531.5 eV which can be related to O-containing species of an organic layer (C–O),^[56] as well as to aluminum oxide layer.^[57] The O_{1s} peak at ~531.5 eV is relatively small compared to the one at ~529 eV in the case of pristine LCO. For the alucone coated LCO samples, the peak at ~531.5 eV is significantly larger than the lattice-O peak at ~529 eV. From this data we get an evidence for the formation of new C–O bonds resulting from the organic precursors, as well as new Al–O bonds formed by the organic-inorganic hybrid layer.

The Co_{2p} scans obtained from coated LCO and uncoated LCO reveal two Co_{2p} peaks at ~794 eV and ~779 eV, corresponding to Co_{2p}_{1/2} and Co_{2p}_{3/2}, respectively. As shown in Figure S13, the alucones coated LCO samples and the pristine LCO show similar Co_{2p} peak positions, indicating no change in the oxidation state of Co during the MLD procedure.

The atomic ratios of the alucone coated and uncoated LCOs calculated from the XPS measurements are shown in Table 1. The results indicate a significant decrease in the percentage of Co atom along with an increase in the percentage of Al and C atoms, corresponding to the coated LCO samples compared to the uncoated LCO. These differences are expected as the deposition of 10–11 nm alucone thin film coating over the LCO surface results in poor accessibility of Co to the X-rays in comparison to the pristine surface.

Table 1. XPS atomic ratios data of coated and uncoated LCO.

Sample	Uncoated LCO	EG/Al coated-LCO	HQ/Al coated-LCO
%Al-2p	–	6.41	4.7
%O-2p	47.58	40.25	34.64
%Co-2p	10.11	4.62	4.87
%C-1s	42.32	48.73	55.79

To give a clear indication on the presence of organic layers, nuclear magnetic resonance (NMR) analysis was carried out. The NMR measurements were first performed on EG/Al and HQ/Al coated LCO samples (Figure 3a). The HQ/Al coated sample indicates two main shifts at 6.7 and 1.7 ppm, associated with the ring protons of the HQ,^[58] and Al-OH moieties.^[59] Deconvolution of the spectrum reveals an additional peak at 0.6 ppm, associated with alkyl methyl groups, possibly originating from the TMA.

No peak is seen in the region of the alcohol proton at 8.6 ppm, suggesting that the –OH protons are removed. However, the ¹H signal from the EG/Al coated LCO sample was very poorly resolved.

Therefore, to obtain a better resolution and improve sensitivity of the EG/Al coat layer, the amount of deposited surface material was increased by performing an identical coating procedure on a high surface area silica powder (SBA15). The ¹H MAS NMR spectrum collected on the EG/Al coated SBA sample is indicated in Figure S14(a), and the peaks are listed on the table in Figure S14(b). The largest two peaks, comprising nearly 70% of the total spectral intensity, are seen at 3.23 and 3.2 ppm, consistent with the chemical shift of the CH₂ in EG.^[60] A significant difference in the line widths of the two peaks (75 vs. 390 Hz, respectively) is indicative of the different constraints that these molecules experience within the coating network; the narrow peak indicates a population of the EG molecules

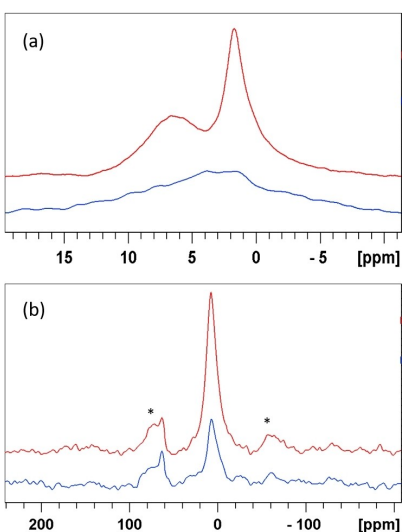


Figure 3. (a) ¹H MAS NMR single pulse spectra of EG/Al (blue) and HQ/Al (red) coated LCO material; (b) ²⁷Al single pulse MAS NMR of HQ/Al (blue) and EG/Al (red) coated LCO. * indicates spinning sidebands.

having increased mobility, while the broad peak indicates greater restriction of motion on the rest of the EG molecules (47%). The peak at -0.4 ppm is assigned to CH_3Al groups from TMA.^[61] The remaining peaks are from $-\text{OH}$ and $-\text{OH}_2^+$ groups on the surface of the SBA material itself.^[62,63] The ^{13}C experiments performed on the coated LCO samples did not yield a discernible signal, even when 99% ^{13}C enriched EG and HQ precursor compounds were used in the coating process.

However, the high surface SBA sample did indicate ^{13}C signal in the EG/Al coated SBA sample. The EG/Al coated SBA spectrum is shown in Figure SI4(c), indicating a peak at 63 ppm associated with the CH_2 signal of EG, and a peak near 0 ppm, which is attributed to CH_3 groups (possibly originating from the TMA) on the SBA surface.^[64] Two different components; a broad one and a narrow one, were discernible in the 63 ppm peak, by processing the data using different line broadening values. The intensities of these two peaks were graphed as a function of contact time in a series of cross-polarization experiments (Figure SI4d). The difference in their build-up time (CP time-constants) is attributable to a kinetic effect, i.e., motional differences in differently coordinated EG molecules,^[65] which corresponds to the broad and narrow CH_2 signals identified in the ^1H data. Thus, approximately half of the EG molecules are more highly constrained within the alucone coating matrix, while the other half exhibit motions (e.g., free rotation around C–C or C–O single bonds). Analogous experiments for the HQ/Al on the SBA15 were not successful, indicating neither ^1H nor ^{13}C signal. This is due to the presence of radicals in the sample, as was confirmed by electron paramagnetic resonance (EPR) (data not shown). The strong exchange interaction between radicals on adjacent quinone rings quenches the NMR signal of the carbon and adjacent proton atoms, rendering them undetectable, although the HQ protons could be observed on in the HQ/Al MLD on LCO material.

The ^{27}Al spectra (Figure 3b) for the two samples were very similar in the exhibited chemical shifts, only indicating differences in peak ratios. Both samples indicated shifts at 63 ppm and 8 ppm. The narrow resonance at 63 ppm is in the region associated with tetrahedrally coordinated aluminum (a AlO_4 structural unit), while the broad high-field resonance at 8 ppm is associated with octahedrally coordinated aluminum, (AlO_6 structural unit)^[66,67] The larger ratio of AlO_6 centers in the EG/Al coated sample indicates a weaker perturbation of the octahedral arrangement of oxygen around the central Al atom by the EG molecules due to their smaller footprint in the mixed layer as compared to HQ.

The Raman spectra of the pristine LCO, the EG/Al coated LCO, and the HQ/Al coated LCO are shown in Figure 4. The main two Raman active vibrational modes at 470.1 cm^{-1} and 582.4 cm^{-1} of E_g and A_{1g} are observed, corresponding to O–Co–O bending and Co–O stretching, respectively.^[68,69] In both alucones coated LCO samples, no significant Raman shifts directly assigned to the organic molecular layer were detected. However, some changes to the LCO shifts are observed in the alucones coated samples suggesting the presence of a coating layer. For the EG/Al coated LCO, both Raman active modes are shifted to higher energy by $\sim 7\text{ cm}^{-1}$, demonstrating a denser

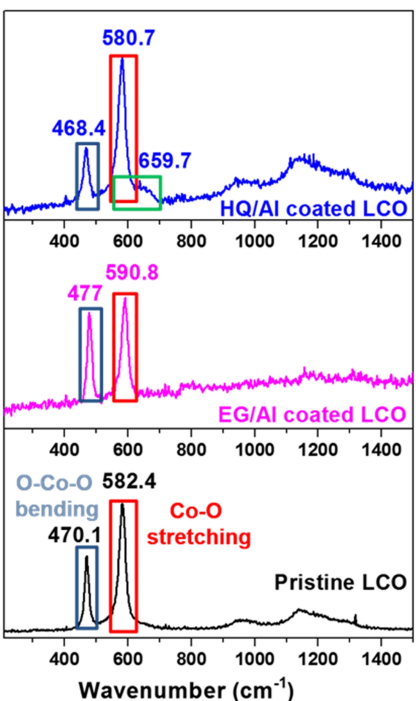


Figure 4. Raman spectra of uncoated LCO (black), 50 MLD cycles of EG/Al thin film coated LCO (pink), and 50 MLD cycles of HQ/Al thin film coated LCO (blue).

arrangement that imparts a restriction on the vibrations.^[70] This denser packing structure can be related to the EG being a small and linear organic molecule. In addition, examining the Raman mode intensity ratios of the EG/Al coated and uncoated LCO reveals that for the EG/Al coated LCO, O–Co–O bending mode is more dominant than Co–O stretching mode. This describes a denser environment, where the population of the stretching mode is decreased due to the higher spatial density from the deposited organic molecule. For the HQ/Al coated LCO, Raman active modes are shifted to lower energy by $\sim 2\text{ cm}^{-1}$ caused by a lower environmental density. In this case, examination of the Raman modes intensity ratios of the HQ/Al coated and uncoated LCO reveals that for the HQ/Al coated LCO, Co–O stretching mode is more dominant than O–Co–O bending mode. Furthermore, a new broad mode is observed at 659.7 cm^{-1} assigned to the HQ molecule.^[71,72] The shape of this peak indicates an amorphous coating. To verify this assignment, we measured a sample with a thicker HQ/Al coating obtained from 100 MLD cycles, demonstrating a higher and sharper peak (shown in Figure SI5).

Next, the crystalline structure of pristine LCO and EG/Al and HQ/Al coated LCO samples were analyzed by XRD (Figure SI6). The XRD patterns of pristine LCO revealed hexagonal LiCoO_2 with cell parameters of $a = 2.81583\text{ \AA}$ and $c = 14.0501\text{ \AA}$, $Z = 3$ [Database #: PDF 50-0653]. Both the EG/Al and HQ/Al coated LCO diffractions remained the same. In all cases, the main XRD peaks appeared at $2\Theta = 18.909^\circ$, 37.43° , and 45.24° , corresponding to $[003]$, $[101]$, and $[104]$ planes, respectively. The absence of any new diffraction lines for the coating itself is in

good agreement with the coatings being very thin and amorphous.

At the next step of this work, we focused on the electrochemistry performance of the coated LCO, and studied the improvement associated with the protection layer of the thin films.

Comparative galvanostatic charge/discharge profiles of the 1st cycle corresponding to the pristine, EG/Al, and HQ/Al coated LCO are shown in Figure SI7(a). All the three materials exhibited similar voltage profiles and specific capacities during the 1st cycle under the same conditions of C/3 rate and a cut-off voltage of 4.45 V. Nevertheless, a pronounced difference in the specific discharge capacity of the coated and uncoated LCO can be seen through the comparative voltage profiles of the pristine LCO, and the alucones coated LCO samples at the 50th cycle (Figure SI7b). Furthermore, the voltage profiles of the uncoated and the alucone coated LCO corresponding to 1st, 25th, 50th, 75th and 100th charge/discharge cycles, recorded at a rate of C/3 and a cut-off voltage of 4.45 V, is shown in Figure 5(a-c). The arrows with dotted lines incorporated in the figures indicate the voltage hysteresis arising during prolonged electrochemical cycling. From the arrows, it can be inferred that as the cycling proceeds, the oxidation processes shift to higher potentials, whereas the reduction peaks shift to lower values. These shifts in potentials and decreased length of redox plateaus with the increasing number of cycles indicate slower kinetics. Moreover, the shifts in the position of the redox processes are attributed to phase transformations and the formation of the SEI with low ionic mobility.^[73,74] As reflected in Figure 5(a), the voltage hysteresis is much more significant in the uncoated LCO, whereas in EG/Al coated LCO (Figure 5c), these deviations in redox potentials are negligible and the redox plateaus remain almost unaltered during prolonged cycling. Moreover, after the 200th cycle (Figure SI7c), both the EG/Al and HQ/Al coated LCO outperform the pristine LCO delivering a specific capacity of 157 mAh/g and 118 mAh/g, respectively, compared to 64 mAh/g of uncoated LCO. After 200 charge/discharge cycles at a rate of C/3 (Figure 5d) EG/Al coated LCO demonstrated capacity retention of ~94% (over 100 cycles) and 86% (over 200 cycles). These results manifested tremendously improved cycling stability compared to both the HQ/Al coated and uncoated LCO that underwent a capacity fading as high as 35% and 65%, respectively, under the same cycling conditions.

In addition to the substantially enhanced discharge capacity, the coated materials also demonstrated much reduced voltage fading compared to the uncoated LCO. Large irreversible capacity, poor columbic efficiency, and severely decreased Li⁺ diffusivity exhibited by LCO when operated above 4.2 V are associated with a series of phase transitions (between O₃ phases and order-disorder transitions) during repeated lithiation and delithiation.^[75,76] Therefore, in contrast to the pristine LCO, the well-maintained voltage plateaus exhibited by the alucone coated material during prolonged cycling manifests the efficacy of the proposed coatings in mitigating the material degradation and compensated Li⁺ diffusion arising from the inevitable phase transitions. We

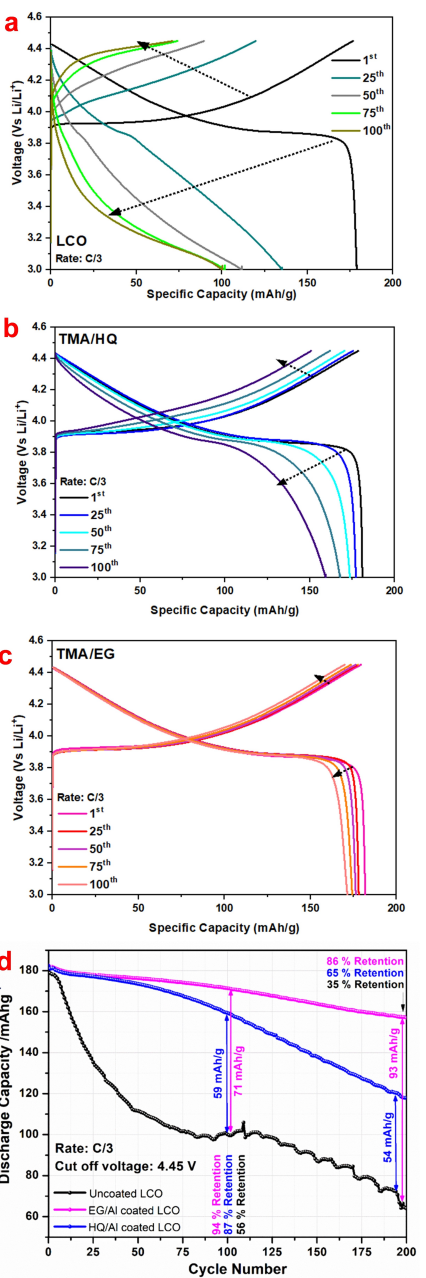


Figure 5. Voltage profiles of 1st, 25th, 50th, 75th, and 100th charge-discharge cycles corresponding to (a) LCO, (b) HQ/Al coated LCO, and (c) EG/Al coated LCO. (d) Cycling performance of uncoated and coated LCO over 200 charge/discharge cycles. Cut off voltage: 4.45 V, at C/3 rate.

anticipate this improvement to the rigid-soft nature of the hybrid organic/inorganic alucone thin film which can overcome the poor plastic deformation characteristics of the inorganic films and suppress the SEI growth by dissipating the inner stress. Additionally, the open structure of the polymeric component is expected to increase the Li⁺ diffusion kinetics which further explains the improved electrochemical performance of the alucone coated sample. In particular, the EG/Al coatings exhibited the best results compared to HQ/Al coatings and the uncoated LCO. This can be explained based on superior ionic conductivity of scaffolds based on EG molecule as

building blocks, owing to Lewis basic nature of O atoms that facilitate Li^+ ionic conductivity. On the other hand, the bulky HQ molecule results in thicker film and reduced oxygen content in the CEI scaffold, leading to retarded electrochemical processes compared to EG.

At a rate of 1 C, the coated and uncoated LCO showed a similar voltage profile for the first cycle (Figure 6a). However, after the 100th charge/discharge cycles (Figure 6b), the voltage plateau of LCO at ~3.9 V disappeared in the case of bare LCO and reduced significantly for the HQ/AI coated LCO, indicating voltage decay and capacity fading. In contrast to pristine LCO and HQ/AI coated LCO, EG/AI coated LCO exhibited a long plateau at 3.9 V, very much like the first cycle. This difference between EG/AI and HQ/AI coated samples was further evident from the cycling performance shown in Figure 6(c), where EG/AI coated LCO exhibited capacity retention of 92%, compared to 58% shown by HQ/AI coated LCO. The enhanced stability achieved by EG/AI coatings compared to HQ/AI coatings at a faster rate of 1 C further supported the hypothesis that the ionic mobility is higher for EG/AI coatings.

To verify the importance of identity and composition of organic species in the CEI,^[77–80] we have compared the rate performance of MLD coated LCO with Al_2O_3 coated LCO, prepared by ALD (by alternating TMA and water precursors). Figure 6(d) represents the discharge capacities of coated and uncoated LCO as a function of C-rate ranging from C/10 to 3 C (C/10, C/5, C/3, 0.8 C, 2 C, 3 C). At all C-rates, the alucone coatings outperformed both the Al_2O_3 coated and pristine LCO. It was also inferred that EG/AI coated LCO shows better performance, mostly at higher C rates which supports the trend of our previous cycling performances.

Next, we have extended the positive voltage of operation for our LCO cathodes to >4.5 V in order to boost the capacity associated with this material. However, it is already well reported that severe structural changes occur when deeper delithiation is attempted by charging LCO above 4.5 V.^[81,82] These changes induce volume changes, accumulation of stress and pulverization of the particles leading to poor stability and limited efficiency. Unambiguously, to achieve a practical cycling life of LCO with >4.5 V cut off voltage, it is critical to limit the phase transformation and associated detrimental structural degradation.

The ability of alucones thin film coatings to stabilize and protect LCO surface and enables charging to higher voltages and gaining higher capacity is presented in Figure 7(d). As shown, increasing the cut off voltage from 4.45 V to 4.52 V causes increase in the initial capacity of 10.1%. The cycling performance of alucones coated LCO cycled at a cutoff voltage of 4.52 V, clearly demonstrates substantially improved cycling stability and significantly mitigated capacity fading and voltage decay at both the tested rates. After 100 cycles, capacity retention of 94% was observed for the EG/AI coated LCO at a rate of C/3, compared to 87% and 54% as shown by the HQ/AI and uncoated LCO, respectively (Figure 7a). Similar improvements in the electrochemical performance of EG/AI coated LCO were observed even at a faster rate of 1 C where EG/AI coated LCO demonstrated impressive capacity retention of 80.7%

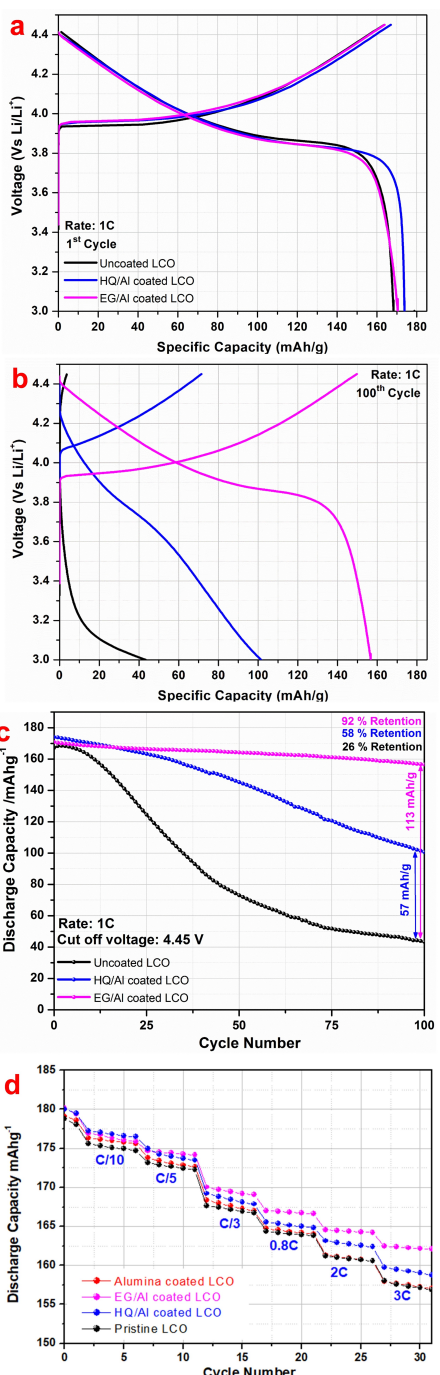


Figure 6. Comparative galvanostatic charge/discharge profiles of pristine LCO (black), EG/AI (pink) coated LCO, and HQ/AI (blue) coated LCO of: (a) the 1st cycle; (b) after 100th cycles; (c) cycling performance evaluated over 200 charge/discharge cycles. Cut off voltage: 4.45 V, at 1 C rate. (d) Cycling rate study of EG/AI coated LCO (pink), HQ/AI coated LCO (blue), Al_2O_3 coated LCO (red), and uncoated LCO (black) as a function of applied C-rates.

compared to 60.5% and 25.2% corresponding to the HQ/AI coated and uncoated LCO, respectively (Figure 7b).

To gain superior capacity and to further test the ability of the coatings to stabilize the LCO surface at more extreme conditions, the cycling performance at a cutoff voltage of 4.55 V was next attempted (Figure 7c). The initial capacities

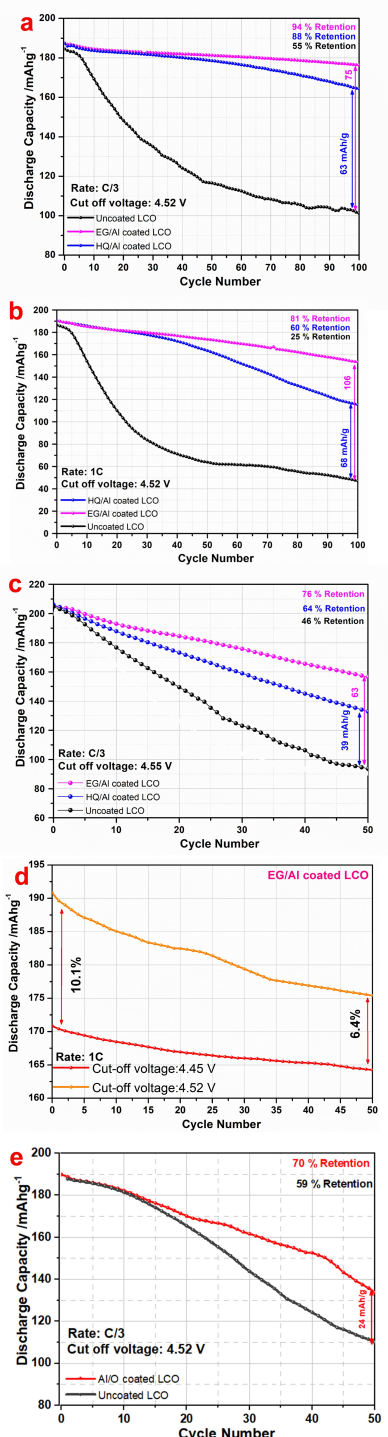


Figure 7. Cycling performance of uncoated LCO (black), EG/AI coated LCO (pink) and HQ/AI coated LCO (blue) at: (a) C/3 rate, 3.0–4.52 V; (b) 1 C rate, 3.0–4.52 V; (c) C/3 rate, 3.0–4.55 V. (d) Comparison of cycling performances of EG/AI coated LCO samples at cut off voltages of 4.45 V vs. 4.52 V at 1 C; (e) Cycling performance obtained of pristine LCO (black) and Al₂O₃ coated LCO (red) at C/3, 3.0–4.52 V.

have shown specific capacities higher than 200 mAh/g for all coated and uncoated LCO. However, after 50 charge/discharge cycles, the uncoated LCO underwent a loss of ~54% of its initial capacity.

The EG/AI coated LCO sample has retained ~76% of its capacity under similar operating conditions. Next, the comparison between the electrochemical performances of the alucone coated LCO and the conventional Al₂O₃ coated LCO was made to infer the role and advantage of hybrid organic-inorganic coatings over inorganic coatings. The cycling performance of Al₂O₃ coated LCO at C/3 rate and cutoff voltage of 4.52 V are presented in Figure 7(e). Based on the comparative studies it can be concluded that though conventional Al₂O₃ is also capable of improving the electrochemical performance of LCO, however, adding organic components to the coating further improves the electrochemical performances which can be attributed to facilitated Li⁺ charge transfer as well as the ability of polymeric component to mitigate the interfacial parasitic reaction.

In order to investigate if there is any phase change after charge/discharge cycling, post-cycled samples at 1 C rate with a cutoff voltage of 4.45 V were tested by XRD. As shown in Figure SI6, the XRD of the post-cycled pristine LCO (Figure SI6a) and the coated samples (Figure SI6b and c) revealed no changes in their Miller planes. However, the XRD of the cycled LCO sample exhibited decrease in the intensity of the peaks corresponding to [101] and [104] post-cycling, as previously reported.^[83,84] The HQ/AI coated LCO also exhibited distorted [003] peak after cycling; however the decrease in the intensity of the [101] and [104] were significantly mitigated. The EG/AI coated LCO has showed the least changes in the XRD patterns after cycling, further supporting the conclusions made from the electrochemical investigations.

To further demonstrate the efficacy of alucones passivation layers, the cycled cathode surface was characterized by HRSEM. The uncoated, EG/AI and HQ/AI coated LCO were taken before and after 100 charge/discharge cycles at 1 C rate with a cutoff voltage of 4.45 V. As shown in Figure SI8, before cycling the slurries prepared from uncoated and alucones coated LCO have similar surface architectures. Nevertheless, after 100 charge/discharge cycles, several cracked and disintegrated particles were observed in the case of the uncoated LCO as shown in Figure 8(a). Such damages over the cathode surfaces are related to structural instability and surface degradation occurring to LCO at high voltages operations (>4.35 V). On the other hand, the EG/AI and HQ/AI coated LCO samples have shown well preserved morphology very similar to the uncycled particles, indicating substantially less structural damage of particle during cycling (Figure 8b and c, respectively). This visual evidence further validate the importance of coatings in improving the electrochemical performance and extending the cycle life.

3. Conclusions

In this work, we demonstrated a straightforward MLD of hybrid organic-inorganic alucone films and tested their efficacy as cathode layer interface for improving electrochemical performances of LCO cathode, specifically for high voltages operations (above 4.5 V vs. Li/Li⁺). The alucone coated LCOs have shown

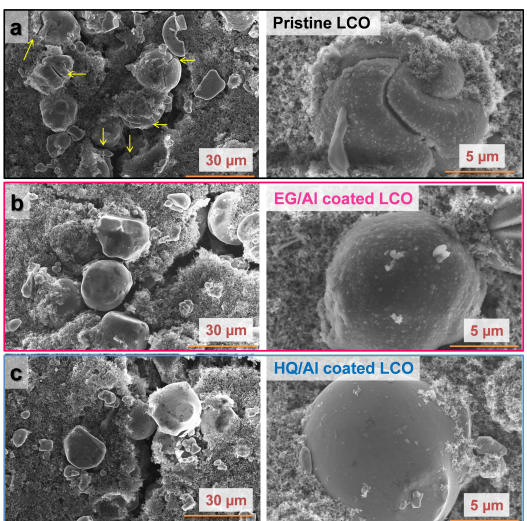


Figure 8. HRSEM images (lower and higher magnification) of post-cycling cathodes after 100 charge/discharge cycles of (a) uncoated LCO, (b) EG/Al coated LCO, and (c) HQ/Al coated LCO. Cut off voltage: 4.45 V, at 1 C rate.

improvements in the electrochemical performances over the uncoated LCO, revealing superior cycling stability, higher specific capacity and greater capacity retention. The EG/Al coated LCO has exhibited the best electrochemical performances, demonstrating capacity retention of 94% at C/3 rate and 92% at 1 C after 100 cycles, at a cut off voltage of 4.45 V. In order to enhance the power density and to gain superior capacity with a stable cycling performance, we have pushed the cut off potential up to 4.55 V. The EG/Al thin films have shown great ability to improve the cycling performance of the LCO up to 56%. Molecular reasons for its superiority were indicated from ssNMR and Raman. In addition, to support the advantages of MLD compared to ALD, rate studies of alucone coated LCO were compared to the conventional Al_2O_3 coated LCO prepared by ALD. As proved, though Al_2O_3 coated LCO have shown higher capacities compared to pristine LCO, the alucones coated LCO samples outperformed the Al_2O_3 coated and uncoated LCO.

We hope the MLD described in this paper can be extended to further hybrid organic-inorganic thin films, due to the variety of available organic precursors. Moreover, we believe the MLD described in this paper can be used as protective thin film coatings over additional electrodes, for gaining electrochemical enhancements in LIBs application.

Experimental Section

Thin films deposition by MLD and ALD. LCO powder (purchased from TOB) was used as the substrate electrode material. Atomic/molecular layer deposition was performed using trimethylaluminum (TMA) as the source for Al atoms, ethylene glycol (EG) and hydroquinone (HQ) as the source for organic moieties, and water as source for O layer (in Al_2O_3 growth). For A/MLD processes, Ultratech savannah 200 ALD was used. The reactor temperatures were maintained at 135 °C, 150 °C, and 200 °C for EG/TMA, HQ/TMA

and TMA/Water procedures, respectively. The EG and HQ precursors were pre-treated by heating to 105 °C overnight under vacuum. The cylinders of EG and HQ were heated and stabilized at 95 °C and 120 °C, respectively. For all A/MLD processes, argon was used as a carrier gas.

For EG/Al thin films growth, MLD cycle consists of 0.03 s pulse time of EG precursor followed by a 15 s of Ar purge, and then by 0.03 s pulse time for TMA followed by a 15 s of Ar purge. For HQ/Al thin film growth, MLD cycle consists of 0.04 s pulse time for HQ precursor followed by a 15 s of Ar purge, and then 0.02 s pulse time for TMA followed by a 15 s of Ar purge. For TMA/Water process, ALD cycle consists of 0.03 s pulse time for TMA precursor followed by a 15 s of Ar purge, and then by 0.03 s pulse time for Water followed by a 15 s of Ar purge.

Characterization methods. The surface of LCO was characterized by a high-resolution scanning electron microscope (HR-SEM, FEI, Magellan 400L). The energy-dispersive X-ray analysis (EDAX) in the HR-SEM was executed by an 80 mm 2X-max detector (Oxford Instruments).

High magnification images of coated and uncoated LCO were taken by transmission electron microscope (TEM, JEM-1400, JEOL, LaB6, accelerating voltage 120 kV, bottom CCD 2×2k camera) and high-resolution transmission electron microscope (HR-TEM, JEM 2100, JEOL, Accelerating Voltage 200 kV, Gatan USC 4000 4×4k camera). TEM samples were prepared on 300-mesh carbon-coated Cu grid.

X-ray photoelectron spectroscopy (XPS) was carried out using Kratos Analytical (England) AXIS-Ultra DLD with monochromatic Al $K\alpha$ (1486.6 eV) X-ray beam radiation. The binding energy of adventitious carbon at 285.0 eV was taken as an energy reference for all the measured peaks.

Nuclear magnetic resonance (NMR) studies for ^1H , ^{13}C and ^{27}Al MAS NMR were conducted on a Bruker Avance 11.4 T magnet spinning at 8–10 kHz in a 4 mm Bruker CP-MAS probe. Additional ^1H measurements were collected on a Bruker Avance 4.7 T magnet spinning at 5–10 kHz in a 3.2 mm probe. The spectra were referenced to TMS (^1H), adamantane (^{13}C) and 1 M aqueous solution of $\text{Al}(\text{NO}_3)_3$ (^{27}Al). The data were fitted using the dmFit NMR processing program.^[66]

The crystalline phase of LCO (coated and uncoated) was studied by powder XRD using a Bruker AXS D8 advance diffractometer with $\text{Cu } K_{\alpha}$ ($\lambda = 1.5418 \text{ \AA}$) operating at 40 kV/40 mA and collected from 20 of 10° to 75°.

Electrochemical measurements. Slurry preparation: The composite electrodes were prepared by spreading a slurry of the following material composition; 80% active material (EG/Al coated LCO, HQ/Al coated LCO, uncoated LCO, Al_2O_3 coated LCO), 10% Super P carbon black, and 10% of 10 wt% PVDF (Polyvinylidene fluoride) solution in NMP (N-methyl pyrrolidone) over Al foil as the current collector. The prepared slurry coated electrodes were then dried overnight at 100 °C followed by calendaring. Using the prepared electrodes, the coin cells were assembled in the Ar filled glove box with Li-metal counter electrodes (\varnothing 14 mm), two Celgard 2500 polypropylene separator (\varnothing 19 mm), and 30 μL of LP57 (1 M LiPF_6 in ethylene carbonate:ethyl methyl carbonate EC:EMC, 3:7).

Specific capacity of LCO of 250 mAh/g was considered for electrochemical calculations. The electrochemical measurements were carried out using BCS-805 battery cycler (Biologic Science instruments) in potential windows of 3.0–4.45 V, 3.0–4.52 V, and 3.0–4.55 V, at various cycling rates. All cells were subjected to electrochemical cycling at 37 °C.

Acknowledgements

L.-S. O. would like to acknowledge the Ministry of Science, Technology & Space, Israel, for the Golda Meir Post-doctoral Scholarships number 1488/3000017538. The authors would like to acknowledge Dr. Ronit Lavi and Prof. Sharon Ruthstein on their help in EPR analyses.

Conflict of Interest

The authors declare no conflict of interest.

Keywords: alucones thin films · atomic layer deposition · LiCoO₂ · Li-ion batteries · molecular layer deposition

- [1] M. Armand, P. Axmann, D. Bresser, M. Copley, K. Edström, C. Ekberg, D. Guyomard, B. Lestriez, P. Novak, M. Petranikova, W. Porcher, S. Trabesinger, M. Wohlfahrt-Mehrens, H. Zhang, *J. Power Sources* **2020**, *479*, 1–26.
- [2] Z. P. Cano, D. Banham, S. Ye, A. Hintennach, J. Lu, M. Fowler, Z. Chen, *Nat. Energy* **2018**, *3*, 279–289.
- [3] L. Han, M. L. Lehmann, J. Zhu, T. Liu, Z. Zhou, X. Tang, C. Heish, A. P. Sokolov, P. Cao, X. C. Chen, et al., *Front. Energy Res.* **2020**, *8*, 1–19.
- [4] J. Hou, M. Yang, D. Wang, J. Zhang, *Adv. Eng. Mater.* **2020**, *1904152*, 1–23.
- [5] H. Fatima, Y. Zhong, H. Wu, Z. Shao, *Mater. Rep. Ene.* **2021**, *1*, 1–19.
- [6] B. Scrosati, J. Garche, *J. Power Sources* **2010**, *195*, 2419–2430.
- [7] M. Armand, J. Tarascon, *Nature* **2008**, *451*, 2–7.
- [8] L. Wang, J. Ma, C. Wang, X. Yu, R. Liu, F. Jiang, X. Sun, A. Du, X. Zhou, G. Cui, *Adv. Sci.* **2019**, *1*, 1–6.
- [9] Y. Lyu, X. Wu, K. Wang, Z. Feng, T. Cheng, Y. Liu, M. Wang, R. Chen, L. Xu, J. Zhou, et al., *Adv. Energy Mater.* **2021**, *11*, 1–29.
- [10] L. Wang, B. Chen, J. Ma, G. Cui, L. Chen, *Chem. Soc. Rev.* **2018**, *47*, 6505–6602.
- [11] Q. Liu, X. Su, D. Lei, Y. Qin, J. Wen, F. Guo, Y. A. Wu, Y. Rong, R. Kou, X. Xiao, et al., *Nat. Energy* **2018**, *3*, 936–943.
- [12] Z. Qi, G. M. Koenig, *Chem. Sel.* **2016**, *1*, 3992–3999.
- [13] Y. Kim, *J. Mater. Sci.* **2013**, 8547–8551.
- [14] X. Liu, J. Zhang, S. Guo, N. Pinna, *J. Mater. Chem. A* **2016**, 1423–1431.
- [15] H. Zhai, Y. Shuai, Y. Wang, K. Chen, *Ionics* **2020**, *26*, 627–637.
- [16] Z. Bi, N. Zhao, L. Ma, Z. Fu, F. Xu, C. Wang, *J. Chem. Eng.* **2020**, *387*, 1–6.
- [17] Y. Zhao, Y. Sha, Q. Lin, Y. Zhong, M. O. Tade, Z. Shao, *ACS Appl. Mater. Interfaces* **2015**, *7*, 1787–1794.
- [18] H. Jeong, S. Lim, S. Chakravarthy, K. Hwan, J. Lee, J. S. Heo, H. Park, *J. Power Sources* **2020**, *451*, 1–6.
- [19] A. Gurung, J. Pokharel, A. Baniya, R. Pathak, K. Chen, B. S. Lamsal, N. Ghimire, W. H. Zhang, Y. Zhou, Q. Qiao, *Sustain. Energy Fuels* **2019**, *3*, 3279–3309.
- [20] C. Li, H. P. Zhang, L. J. Fu, H. Liu, Y. P. Wu, E. Rahm, R. Holze, H. Q. Wu, *Electrochim. Acta* **2006**, *51*, 3872–3883.
- [21] Z. Chen, Y. Qin, Y. Sun, *J. Mater. Chem.* **2010**, 7606–7612.
- [22] C. Cai, Y. Wang, *Materials (Basel)* **2009**, *2*, 1205–1238.
- [23] A. T. Appapillai, A. N. Mansour, J. Cho, Y. Shao-horn, *Chem. Mater.* **2007**, *19*, 5748–5757.
- [24] Y. Zhao, L. Zhang, J. Liu, K. Adair, F. Zhao, Y. Sun, T. Wu, X. Bi, K. Amine, J. Lu, et al., *Chem. Soc. Rev.* **2021**, *50*, 3889–3956.
- [25] Y. Zhao, K. Adair, X. Sun, *Matter* **2019**, *1*, 1119–1126.
- [26] X. Meng, *J. Mater. Res.* **2021**, *36*, 2–25.
- [27] A. S. Asundi, J. A. Raiford, S. F. Bent, *ACS Energy Lett.* **2019**, *4*, 908–925.
- [28] L. Ma, R. B. Nuwayhid, T. Wu, Y. Lei, K. Amine, J. Lu, *Adv. Mater. Interfaces* **2016**, *3*, 1–15.
- [29] C. Hirschberg, N. S. Jensen, J. Boetker, A. Ø. Madsen, T. O. Kaäriäinen, M. L. Kaäriäinen, P. Hoppu, S. M. George, M. Murtomaa, C. C. Sun, et al., *Org. Process Res. Dev.* **2019**, *23*, 2362–2368.
- [30] M. J. Young, N. M. Bedford, A. Yanguas-Gil, S. Letourneau, M. Coile, D. J. Mandia, B. Aoun, A. S. Cavanagh, S. M. George, J. W. Elam, *ACS Appl. Mater. Interfaces* **2020**, *12*, 22804–22814.
- [31] J. Azadmanjiri, J. Wang, C. C. Berndt, A. Yu, *J. Mater. Chem. A* **2018**, *6*, 3824–3849.
- [32] M. D. Groner, F. H. Fabreguette, J. W. Elam, S. M. George, *Chem. Mater.* **2004**, *16*, 639–645.
- [33] J. W. Elam, M. D. Groner, S. M. George, *Rev. Sci. Instrum.* **2002**, *73*, 2981–2986.
- [34] X. Zhang, I. Belharouak, L. Li, Y. Lei, J. W. Elam, A. Nie, X. Chen, R. S. Yassar, R. L. Axelbaum, *Adv. Energy Mater.* **2013**, *3*, 1299–1307.
- [35] X. Meng, *J. Mater. Chem. A* **2017**, *5*, 18326–18378.
- [36] H. Van Bui, F. Grillo, J. R. Van Ommeren, *Chem. Commun.* **2017**, *53*, 45–71.
- [37] A. Muriqi, M. Nolan, *Dalton Trans.* **2020**, *49*, 8710–8721.
- [38] J. P. Niemelä, N. Rohbeck, J. Michler, I. Utke, *Dalton Trans.* **2020**, *49*, 10832–10838.
- [39] B. C. Welch, O. M. McIntee, A. B. Ode, B. B. McKenzie, A. R. Greenberg, V. M. Bright, S. M. George, *J. Vac. Sci. Technol. A* **2020**, *38*, 0524091–05240910.
- [40] S. Chaudhury, E. Wormser, Y. Harari, E. Edri, O. Nir, *ACS Appl. Mater. Interfaces* **2020**, *12*, 53356–53364.
- [41] B. H. Lee, B. Yoon, V. R. Anderson, S. M. George, *J. Phys. Chem. C* **2012**, *116*, 3250–3257.
- [42] S. Hollevoet, K. B. Gandrud, M. Y. Timmermans, B. Put, Y. El Ajouri, K. Van de Kerckhove, C. Detavernier, M. Mees, P. M. Vereecken, *Adv. Mater. Interfaces* **2019**, *1*, 6.
- [43] B. Gong, Q. Peng, G. N. Parsons, *J. Phys. Chem. B* **2011**, *115*, 5930–5938.
- [44] S. M. George, B. Yoon, A. A. Dameron, *Accon. Chem. Res.* **2009**, *42*, 498–508.
- [45] B. Yoon, Y. Lee, A. Derk, C. Musgrave, S. George, *ECS Trans.* **2019**, *33*, 191–195.
- [46] L. Chen, Z. Huang, R. Shahbazian-Yassar, J. A. Libera, K. C. Klavetter, K. R. Zavadil, J. W. Elam, *ACS Appl. Mater. Interfaces* **2018**, *10*, 7043–7051.
- [47] D. W. Choi, M. Yoo, H. M. Lee, J. Park, H. Y. Kim, J. S. Park, *ACS Appl. Mater. Interfaces* **2016**, *8*, 12263–12271.
- [48] Y. S. Park, H. Kim, B. Cho, C. Lee, S. E. Choi, M. M. Sung, J. S. Lee, *ACS Appl. Mater. Interfaces* **2016**, *8*, 17489–17498.
- [49] J. W. Dumont, S. M. George, *J. Phys. Chem. C* **2015**, *119*, 14603–14612.
- [50] Y. Lee, B. Yoon, A. S. Cavanagh, S. M. George, *Langmuir* **2011**, *27*, 15155–15164.
- [51] A. A. Dameron, D. Seghete, B. B. Burton, S. D. Davidson, A. S. Cavanagh, J. A. Bertrand, S. M. George, *Chem. Mater.* **2008**, *20*, 3315–3326.
- [52] E. Kazヤk, M. Shin, W. S. Lepage, T. H. Cho, N. P. Dasgupta, *Chem. Commun.* **2020**, *56*, 15537–15540.
- [53] Y. Zhao, X. Sun, *ACS Energy Lett.* **2018**, *3*, 899–914.
- [54] W. Xiao, D. Y. Hui, C. Zheng, D. Yu, Y. Y. Qiang, C. Ping, C. L. Xiang, Z. Yi, *Nanoscale Res. Lett.* **2015**, *1*, 1–10.
- [55] S. Verdier, L. El Ouatani, R. Dedryvère, F. Bonhomme, P. Biensan, D. Gonbeau, *J. Electrochem. Soc.* **2007**, *154*, 1088.
- [56] J. Landoulis, M. J. Genet, S. Fleith, Y. Touré, I. Liascukiene, C. Méthivier, P. G. Rouxhet, *Appl. Surf. Sci.* **2016**, *383*, 71–83.
- [57] N. Kumar, K. Biswas, *J. Mater. Res. Technol.* **2019**, *8*, 63–74.
- [58] "Chemical Book: Hydroquinone," can be found under https://www.chemicalbook.com/SpectrumEN_123-31-9_1H_NMR.htm, 2017.
- [59] W. J. Malfait, X. Xue, *Solid State Nucl. Magn. Reson.* **2010**, *37*, 60–68.
- [60] "Chemical Book: Ethylene Glycol," can be found under https://www.chemicalbook.com/SpectrumEN_107-21-1_1H_NMR.htm, 2017.
- [61] I. Edition, R. Federation, *Russ. Chem. Bull., Int. Ed.* **2011**, *60*, 1461–1468.
- [62] Z. Li, C. Rieg, A. K. Beurer, M. Benz, J. Bender, C. Schneck, Y. Traa, M. Dyballa, M. Hunger, *Adsorption* **2021**, *27*, 49–68.
- [63] G. Hartmeyer, C. Marichal, B. Lebeau, S. Rigolet, P. Caullet, J. Hernandez, *J. Phys. Chem. C* **2007**, *111*, 9066–9071.
- [64] H. Reich, "NMR Spectroscopy," can be found under https://organicchemistrydata.org/hansreich/resources/nmr/?index=nmr_index%2F13C_shift.html, 2020.
- [65] C. Martineau, F. Taulelle, M. Haouas, *PATAI'S Chem. Funct. Groups* **2016**, 1–51.
- [66] D. Massiot, F. Fayon, M. Capron, I. King, S. Le Calve, B. Alonso, J. O. Durand, B. Bujoli, Z. H. Gan, G. Hoatson, *Magn. Reson. Chem.* **2002**, *40*, 70–76.
- [67] M. Duffiet, M. Blangero, P. E. Cabelguen, K. S. Song, F. Fauth, C. Delmas, D. Carlier, *Inorg. Chem.* **2020**, *59*, 2890–2899.
- [68] E. Flores, P. Novák, E. J. Berg, *Front. Energy Res.* **2018**, *6*, 1–16.
- [69] C. M. Julien, A. Mauger, *AIMS Mater. Sci.* **2018**, *5*, 650–698.
- [70] H. W. Thompson, W. T. Cave, *Trans. Faraday Soc.* **1951**, *47*, 946–950.
- [71] R. Cabrera-Alonso, E. Guevara, M. G. Ramírez-Elías, B. Moncada, F. J. González, *J. Nanophotonics* **2019**, *13*, 1.

- [72] M. Kubinyi, F. Billes, A. Grofcsik, G. Kereszty, *J. Mol. Struct.* **1992**, *266*, 339–344.
- [73] N. Mohamed, N. K. Allam, *RSC Adv.* **2020**, *21*, 21662–21685.
- [74] J. Zhang, Q. Li, Y. Wang, J. Zheng, X. Yu, H. Li, *Energy Storage Mater.* **2018**, *14*, 1–7.
- [75] Q. Liu, X. Su, D. Lei, Y. Qin, J. Wen, F. Guo, Y. A. Wu, Y. Rong, R. Kou, X. Xiao, et al., *Nat. Energy* **2018**, *3*, 936–943.
- [76] H. Ben Yahia, M. Shikano, H. Kobayashi, *Chem. Mater.* **2013**, *2*, 3687–3701.
- [77] S. Liu, D. Liu, S. Wang, X. Cai, K. Qian, F. Kang, B. Li, *J. Mater. Chem. A* **2019**, *7*, 12993–12996.
- [78] Z. Yu, Y. Cui, Z. Bao, *Cell Rep. Phys. Sci. Rep. Phys. Sci.* **2020**, *1*, 1–19.
- [79] K. Edström, T. Gustafsson, J. O. Thomas, *Electr. Acta* **2004**, *50*, 397–403.
- [80] X. T. Wang, Z. Y. Gu, W. H. Li, X. X. Zhao, J. Z. Guo, K. Di Du, X. X. Luo, X. L. Wu, *J. Chem. Asian.* **2020**, *15*, 2803–2814.
- [81] N. Nitta, F. Wu, J. T. Lee, G. Yushin, *Mater. Today* **2015**, *18*, 252–264.
- [82] J. P. Pender, G. Jha, D. H. Youn, J. M. Ziegler, I. Andoni, E. J. Choi, A. Heller, B. S. Dunn, P. S. Weiss, R. M. Penner, et al., *ACS Nano* **2020**, *14*, 1243–1295.
- [83] A. Zhou, Y. Lu, Q. Wang, J. Xu, W. Wang, X. Dai, J. Li, *J. Power Sources* **2017**, *346*, 24–30.
- [84] A. Zhou, Q. Liu, Y. Wang, W. Wang, X. Yao, W. Hu, L. Zhang, X. Yu, J. Li, H. Li, *J. Mater. Chem. A* **2017**, *24*, 361–24370.

Manuscript received: July 6, 2021
Revised manuscript received: August 10, 2021
Accepted manuscript online: August 11, 2021
Version of record online: August 23, 2021